J. Fluid Mech. (1998), *vol.* 358, *pp.* 87–106. Printed in the United Kingdom

Measurements of the temperature field of mushy and liquid regions during solidification of aqueous ammonium chloride

By T. H. SOLOMON AND R. R. HARTLEY
Department of Physics, Bucknell University, Lewisburg, PA 17837, USA

(Received 2 August 1996 and in revised form 29 October 1997)

Experiments are conducted to study the solidification from below of aqueous ammonium chloride. Thermochromic liquid crystal paints are used to visualize the temperature field simultaneously in both the liquid and the mushy layers. In a quasi-two-dimensional cell (thickness 10 mm), mushy-layer and boundary-layer convection are revealed as bumps in isotherms within and above the mushy layer, respectively. The onset, growth and decay of these convective modes are measured by monitoring the progression of the bumps during an experiment. The small-wavelength boundary-layer mode is short-lived (approximately 20–30 min), whereas the larger-wavelength mushy-layer mode survives for several hours, dominating the flow even long after the growth has stopped. Experiments in a Hele-Shaw cell (thickness 2.0 mm) enable simultaneous visualization of both the temperature field and the solid fraction. A coarsening mechanism is observed in which the flow spontaneously changes, reducing the strength of plume convection in one of the channels, and leading to growth of dendrites into the channel. An oscillatory convective mode is also observed, perhaps an indication of one of the oscillatory modes recently predicted by Chen, Lu & Yang (1994) and by Anderson & Worster (1995).

1. Introduction

The solidification of binary alloys from a melt is a dynamical system in which fluid flows couple with the growth process. An important manifestation of this coupling is the formation of 'freckles' in metal casts that can significantly compromise the strength of the material. These freckles are caused by focused, vertical, convective flows that produce long channels or 'chimneys', as was first shown experimentally by McDonald & Hunt (1970) and by Copley *et al.* (1970). An understanding of the interaction between solidification and fluid flows is therefore important for producing better quality materials.

Chimneys originate in mushy layers composed of solid dendrites with liquid in the interstitial spaces. A mushy layer is a reactive porous medium in which fluid flows affect growth and dissolution (Huppert 1990; Worster 1991). Supersaturated fluid falling through the mush enhances dendritic growth, decreasing the permeability in down-flow regions. On the other hand, depleted fluid rising through the mushy layer causes dissolution of dendrities, increasing the permeability in up-flow regions. The increased permeability enhances and focuses the flow into narrow channels which develop into well-defined chimneys.

Mathematical models were developed by Hills, Loper & Roberts (1983), Fowler

(1985), and Worster (1991) to describe the temperature and concentration fields in the mushy layer and in the compositional boundary layer directly above the mush–liquid interface. (See Worster 1997 for a review of the literature on this subject.) A detailed linear stability analysis by Worster (1992) identified two instability mechanisms which can lead to compositional convection when a solid is grown from below. The 'boundary-layer' mode (salt-finger convection) is a small-wavelength flow confined predominately to the compositional boundary layer. The larger-wavelength 'mushy-layer' mode originates from within the mushy layer, but penetrates as well into the liquid region. The mushy-layer mode is predicted to be responsible for the narrow vertical plumes and their associated chimneys. Emms & Fowler (1994) extended the analysis to consider the stability of the mushy layer in the presence of salt-finger convection in the boundary layer. They found that salt-finger convection has little effect on the stability of the mushy-layer mode. Weakly nonlinear studies by Amberg & Homsey (1993), on the other hand, characterized the instability of the mushy-layer mode to be subcritical in most situations, and they speculated that although the two modes are predominately independent, the mushy-layer mode might be triggered initially by convection in the boundary layer. Nonlinear theories by Anderson & Worster (1996) and by Worster, Anderson & Schulze (1996) have more fully characterized the flow and temperature fields associated with the mushy-layer mode once initiated.

Experimental studies of chimney formation have recently been focused on the solidification of ammonium chloride (NH_4Cl) from solution. Because of its proclivity for producing chimneys, NH_4Cl solidification processes are widely considered to be good analogues to those for metallic alloys, such as lead–tin, aluminium–copper and nickel–aluminium, as discussed by Huppert (1990). NH_4Cl solutions are much easier to handle than their metallic counterparts, and visualization of the solidification patterns is possible in real time since the liquid phase is transparent.

Recent experiments by Chen & Chen (1991), Tait & Jaupart (1992), Tait, Jahrling & Jaupart (1992), and Chen, Lu & Yang (1994) verified that plume convection and chimney formation result from instabilities of the mushy layer. These experiments identified a critical mush thickness for the onset of chimneys. Sample & Hellawell (1984) found that perturbations due to a pipette could trigger the formation of chimneys, and provided the first indications that the mushy-layer mode may be subcritical, triggered by disturbances from convection in the compositional boundary layer.

Quantitative measurements of mushy-layer properties during chimney formation is difficult because the forest of dendrites makes the region opaque. Despite this obstacle, Chen (1995) made measurements of the solid fraction in a growing NH_4Cl mushy layer using X-ray tomography. Dye techniques were also used to confirm that up-flow regions associated with the mushy-layer mode are focused into tight channels, whereas the down-flow regions are very broad and diffuse. Chen *et al.* (1994) made measurements of the temperature and concentration at fixed points in the mushy layer, demonstrating that the fluid in the mushy layer is in thermodynamic equilibrium. However, no direct measurements have yet been obtained of the velocity or temperature fields in a growing mush. Measurements of these fields are required for detailed comparison with theory and to gain a complete characterization of the flows in a growing mush.

In this paper, we present direct measurements of the temperature field during the solidification of NH_4Cl from aqueous solution. Thermochromic liquid crystals (TLCs) painted on the inner wall of the apparatus change colour with temperature, providing visualization of temperature isotherms in both the mushy and liquid layers.

In addition to providing the first temperature field measurements in a growing mushy layer, these experiments also provide the most direct characterization of the velocity field to date, since flows in the system are revealed as distortions in the isotherms. By measuring these distortions as a function of time, the time evolution of both the mushy and boundary layer flows can be determined quite precisely.

Two sets of experiments are described. The first experiments are conducted in a quasi-two-dimensional configuration: the experimental cell is 10 mm thick, thicker than the typical width of convective plumes emanating from chimneys (approximately 5 mm), but thin enough such that the temperature field mapped on the side reflects the internal field in the mushy layer. These experiments are complemented by two-dimensional studies in a Hele-Shaw cell with a thickness of 2.0 mm. The thin geometry of the Hele-Shaw cell allows direct visualization of the growth and decay of chimneys within the mushy layer simultaneously with the temperature field.

Detailed measurements are made of the growth, decay and interactions of the mushy- and boundary-layer convective modes. The experiments provide direct tests of theoretical predictions about the penetration of the modes into the mushy and liquid regions, along with their time scales. In addition, a coarsening (wavelength-selection) mechanism is identified in which a reversal in the convective flow occurs, allowing dendrites to grow into the chimneys and seal them off. An oscillatory state is also observed in which two chimneys and their associated plumes oscillate out of phase.

The experimental apparatus and measurement techniques are described in §2. The results of the experiments with the quasi-two-dimensional (10 mm thick) cell are described in §3. The two-dimensional (2.0 mm) experiments are described in §4. The experiments are summarized and discussed in §5.

2. Experimental techniques

2.1. *Apparatus and fluids*

The solution used in these experiments is 26.5% NH_4Cl by weight in water, with a liquidus temperature of 17°C. (See Chen & Chen 1991 for a plot of the liquidus curve for NH_4Cl solutions.) The fluid is contained within a cell ('inner cell') constructed of $\frac{1}{4}$ in. thick, optically clear Plexiglas sidewalls and bounded above and below by copper plates (figure 1). (The copper plates are sprayed with a light coating of polyurethane varnish to inhibit chemical reactions with the NH_4Cl.) A gap with height 8.0 cm and width 16.0 cm inside the cell forms the experimental region. The gap thickness (thickness of the NH_4Cl solution) is either 10 mm or 2.0 mm. The entire inner cell is incorporated into a Plexiglas outer box, as shown in the figure.

The apparatus is designed to enable independent temperature control at the two copper plates (the top and bottom surfaces) and at the Plexiglas sidewalls. The bottom temperature is regulated with a 50% ethylene glycol–water mixture that circulates between a Neslab temperature-controlled bath (accuracy 10 mK) and a box attached to the bottom copper plate of the cell. The upper-plate temperature is controlled with a thin resistance-element heater attached to a Tronac temperature controller (accuracy 10 mK). Finally, the sidewall temperatures are maintained by a second Neslab bath that pumps fluid through the outer Plexiglas box surrounding the inner cell.

In a typical experiment, the outer box is allowed to reach its target temperature before the run begins. (Verification that the temperature has equilibrated is very

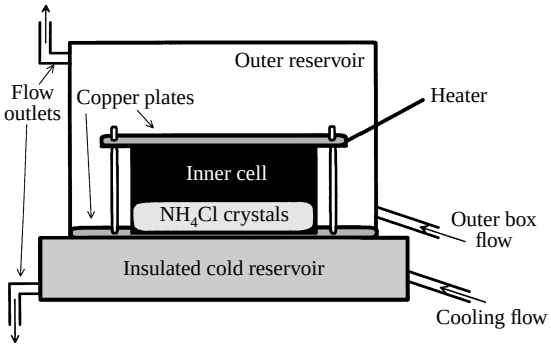

FIGURE 1. Diagram of experimental apparatus. The solidification occurs inside the inner cell, whose bottom temperature is controlled by a cooling flow pumped through the insulated cold reservoir. The top temperature is controlled by the heated copper plate. The temperatures at the sides of the inner cell are controlled by flow through the outer box.

straightforward with the technique described in the next subsection.) The chosen outer box temperature T_o can have a profound effect on the solidification process. If T_o is appreciably above the liquidus temperature, then growth of NH_4Cl proceeds sluggishly, and the long-term mushy layer height is limited. On the other hand, if T_o is appreciably below the liquidus temperature, then NH_4Cl crystals form away from the bottom of the cell. In the 2.0 mm cell, these crystals can grow and get stuck, reducing the flow in the liquid region and depleting some of the NH_4Cl. In both the 2.0 and 10 mm cells, runs with low T_o are also accompanied sometimes by a 'snow' of seed crystals that can produce very permeable aggregation patterns which can dramatically alter the mushy-layer dynamics. (Experiments are currently in progress to address these effects.)

For the experiments reported in this paper, T_o is chosen to be close to the liquidus temperature: T_o is either 10.0 or 15.0°C. The temperature of the bottom copper plate T_b is typically -10°C at the start of the run, rising to approximately -8°C during the first 30 minutes. The upper plate is held at a temperature $T_u = 20.0$°C. All of these temperatures are above the eutectic temperature, so the water never freezes and the solid region is entirely a mushy layer. Since $T_b < T_u$, the thermal stratification is stable. Convection in these experiments is therefore due entirely to compositional variations caused by the growing NH_4Cl.

2.2. *Temperature field measurement*

A technique using thermochromic liquid crystal (TLC) paint enables imaging of a two-dimensional map of the temperature field. This technique is illustrated in figure 2, which shows an exploded view of the inner cell. The TLC paint (obtained from Hallcrest Products, Glenview, IL) is an aqueous acrylic-based coating containing a slurry of microencapsulated cholesteric liquid crystals. Five different TLC paints are mixed together, each with its own 'colour play profile' (see table 1 for these profiles). Five or six coats of this mixture are applied to the inside surface of one of the 8 cm × 16 cm Plexiglas side pieces. When the TLC paint dries, a coat of black paint is applied. The surface is then laminated with mylar tape, which becomes one of the inner surfaces of the inner cell. Only the mylar tape and black paint separate the liquid crystals from the flow; consequently, the response time for temperature visualization is only a few seconds.

Despite the fact that the fluid is motionless along the sidewalls (due to the no-

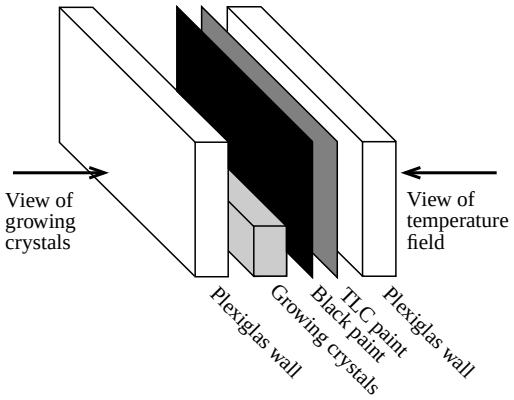

FIGURE 2. Exploded view of inner cell, illustrating the thermochromic liquid crystal technique for temperature visualization.

Paint	Visible start	Red start	Green start	Blue start
1	0.5	0.9	1.4	2.4
2	4.6	4.8	5.2	6.0
3	8.2	8.9	9.4	10.4
4	12.6	12.8	13.4	14.3
5	16.7	17.0	17.5	18.4

TABLE 1. Starting temperatures of the five TLC paints mixed together in these experiments (in °C).

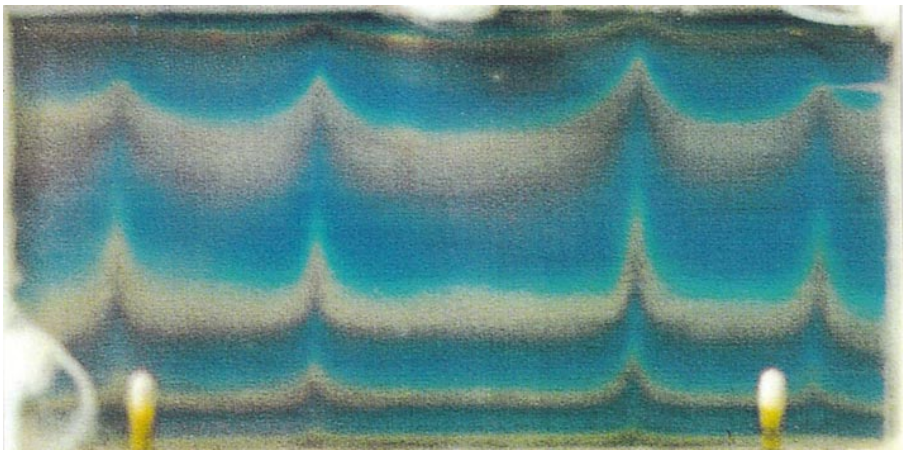

FIGURE 3. Visualization of the temperature field using thermochromic liquid crystal (TLC) paints; 10 mm cell thickness, $T_o = 10.0$°C, 120 min after start of run. Five isotherms are clearly visible as coloured bands in this image (1, 5, 9, 13 and 17°C, from bottom), and plume convection is revealed as upward bumps in these isotherms. (Four plumes are clearly visible.) The mush–liquid interface is just below the third isotherm. The same TLC image is shown in figure 4(f), along with the growing NH_4Cl layer.

slip condition), the TLC paint still responds to the flow in the interior due to the rapid diffusion of heat across the narrow gap. The thermal diffusion time is given by $\tau = l^2/\kappa$, where l is half the cell thickness and κ is the thermal diffusivity of water. For the 2.0 mm cell, $\tau \approx 5$ s, much shorter than typical time scales for the flow (> 100 s).

For the 10 mm cell, $\tau \approx 100$ s for flows in the centre of the cell, comparable to the fastest time scales of the flow. In the experiments shown using this cell, though, the plumes are all situated near the side with the TLC paint, so the thermal diffusion time drops to ≈ 20 s, again much shorter than typical time scales for the flow. Because the TLC paint is on the inside wall of the cell, the amount of heat exchanged with the fluid is negligible over time scales comparable to those of the convective flows. The thermal diffusion time characterizing exchange of heat through the $\frac{1}{4}$ in. thick sidewalls is several orders of magnitude longer than that for conduction across the fluid layer, so the sidewalls can be considered to be good insulators.

The painted Plexiglas provides a black background for visualization of the growing NH_4Cl crystals, which are imaged with a monochrome CCD video camera. The temperature field is observed simultaneously with a second video camera from the opposite side, looking through the Plexiglas sidewall with the TLC paint. Images from the two video cameras are digitized into separate frame buffers, and the image from the solid side is flipped horizontally to enable easy comparison between the growing solid and the temperature isotherms. In all the images shown in this article, the image from the TLC side is displayed directly below that from the solidification side.

The images taken from the TLC side are contour maps of the temperature field at the inner surface of the painted Plexiglas sidewall. An example of a colour photograph of a TLC image showing four fully developed plumes is shown in figure 3. Five isotherms are visible as coloured bands, corresponding to temperatures of 1, 5, 9, 13 and 17°C. Note that visualization of the isotherms is possible both in the liquid and the mushy layer regions (the 1 and 5°C isotherms are both below the mush–liquid interface).

An advantage of using a mixture of TLC paints is that multiple isotherms can be obtained with standard monochrome imaging. A black and white version of figure 3 is shown in figure 4(*f*). The isotherms appear as bright bands in a monochrome image. The isotherms are traced by a program that takes a vertical cut through the bright band and fits the pixel intensities to a parabola. The location of the peak of the parabola is taken to be the centre of the isotherm. The results of this analysis are illustrated in figure 4 as thin, white/black lines superimposed on the images of the growing NH_4Cl mushy layer. The parabolic fitting technique is accurate only in regions where the bright bands in the TLC images are less than 1 cm thick in the vertical direction. Where the bands are thicker than 1 cm (see e.g. the top isotherm in figure 4*a*), the isotherm centres are estimated by hand. (None of the estimated isotherms are used in any of the quantitative analyses later in the paper.)

In regions where the bands are narrow, the parabolic fitting technique enables extremely precise measurements of deviations in the isotherm height. Since the fits allow sub-pixel interpolation, the isotherm centres are measured to a precision of approximately 1/10 the pixel resolution. In these experiments, this translates to a resolution of approximately 40 μm (1/2000 the cell height). With this precision, it is possible to identify the onset of plume convection even when the isotherm bumps are too small to be seen visually.

3. Experiments with 10 mm cell

The growth of the NH_4Cl layer in the 10 mm thick cell is typically accompanied by the eventual formation of 3 or 4 somewhat regularly spaced chimneys. The chimneys grow to a cross-sectional diameter of approximately 5 mm, smaller than the thickness of the cell, so they can only be visualized in the solidification pattern by the caps that

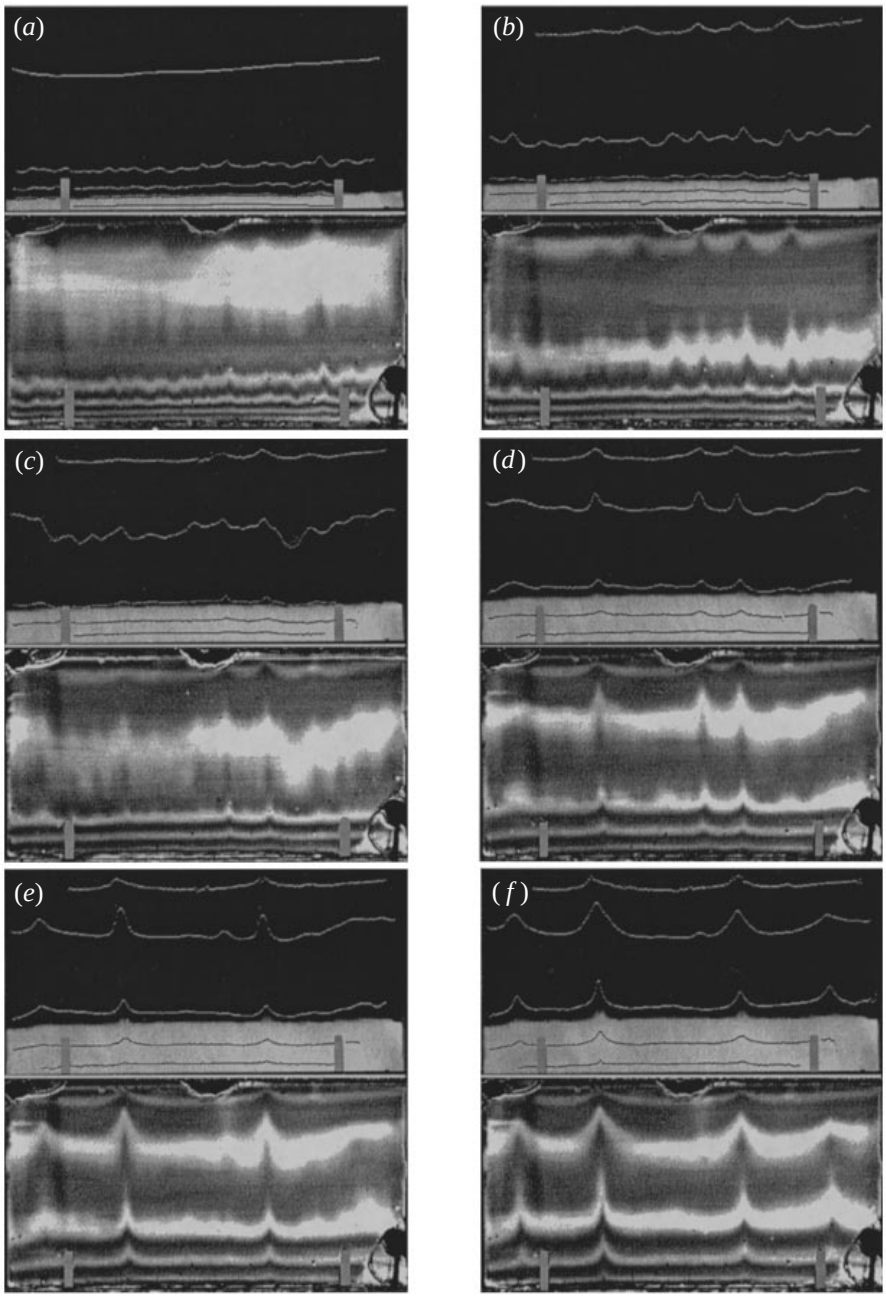

FIGURE 4. Sequence showing solidification in a 10 mm thick cell; $T_o = 10.0°C$. In each frame, the top image shows the growing NH_4Cl mushy layer, and the bottom shows the corresponding TLC image (temperature field). The isotherm centres (determined by parabolic fits) are superimposed on the images of the growing NH_4Cl for reference. The grey rectangles correspond to screws that obstruct the bottom of each image near the left and right sides. Time after start of run: (*a*) 10 min; (*b*) 20 min; (*c*) 30 min; (*d*) 51 min; (*e*) 70 min; (*f*) 120 min.

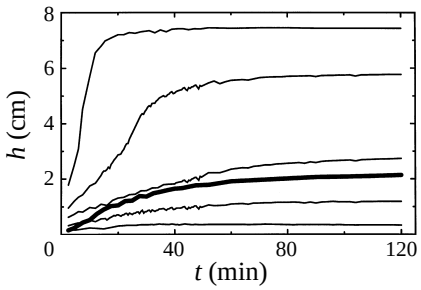

FIGURE 5. Average height of the five isotherms versus time, plotted with the interface height (thick line); 10 mm cell, $T_o = 10.0°C$. The five thin lines represent (respectively, from the bottom) the 1, 5, 9, 13 and 17°C isotherms.

form at their exits. In the run shown in figures 3 and 4 the chimneys are predominately in the back half of the cell, adjacent to the sidewall with the TLC paint. As a result, the TLC images are particularly sensitive to mushy-layer convection.

The sequence of images shown in figure 4 correspond to a run with $T_o = 10.0°C$. Small-wavelength undulations are visible in the isotherms above the mush-liquid interface during the first 30 minutes (figure 4*a–c*), an indication of boundary-layer convection. These undulations fade after approximately 30 minutes, after which only three pronounced bumps are visible (figure 4*d*). These bumps, present both in the liquid and mushy regions, are due to mushy-layer convection, which leads to the formation of chimneys, evidenced by chimney caps that first appear approximately 50 minutes after the start of the run (figure 4*d*). One of the plumes decays after 50 minutes, and two additional plumes grow at the left and right edges. After two hours (figure 4*f*), the flow is completely dominated by four plumes, which penetrate all the way from the bottom of the mushy layer to the top of the liquid region.

The mush/liquid interface can be approximated as an isotherm in most of these images (and those presented later in the paper), consistent with the approximations used in theoretical analyses of mushy-layer flows. The approximation breaks down in two situations: (i) early in the runs, when the growth can be uneven due to variations in nucleation; and (ii) directly above the chimneys where the plume flows can cause sharp kinks in the isotherms.

A plot of the average height of the isotherms versus time is shown in figure 5, along with the liquid–mush interface height (bold line). Over most of the run (after the first 10 minutes), the bottom two isotherms (1 and 5°C) are within the mushy layer, while the 9, 13 and 17°C isotherms are in the liquid region. The 9°C isotherm is located just above the liquid–mush interface throughout the run, so it is sensitive to fluid motion in the compositional boundary layer. During the first 20–30 minutes of the run, the mushy layer grows rapidly, and the average temperature in the liquid region drops from approximately 17°C down to approximately 11°C, as seen by the movement of the 13 and 17°C isotherms. After approximately 30 minutes, the growth of the mushy layer slows as the NH_4Cl concentration drops toward the saturation point, and the mushy-layer interface levels off eventually at a height of 2.2 cm.

The evolution of the flow in the mushy and boundary layer regions is best displayed by space–time plots of the 5°C and 9°C isotherms (figures 6 and 7, respectively). In these plots, only the central region between the two outer box screws is displayed, so the two chimneys that develop at the left and right ends of the cell are excluded.

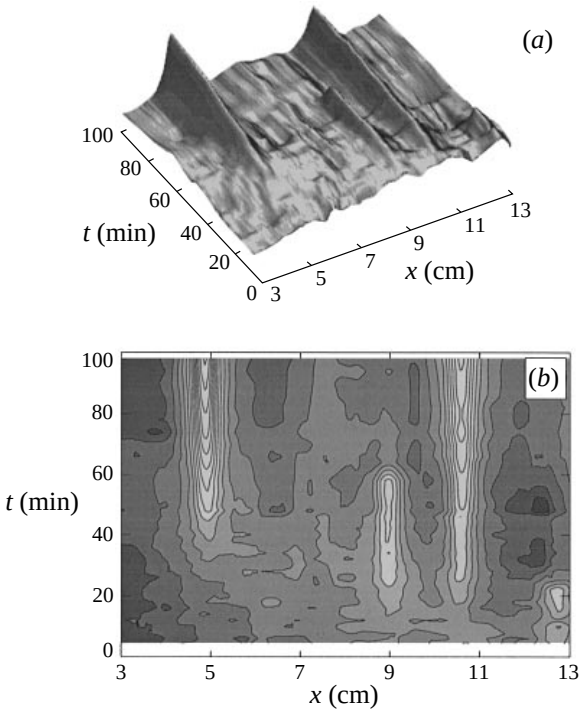

FIGURE 6. Space–time plots of 5°C isotherm (second from bottom in figure 4 and inside the mushy layer); 10 mm cell thickness, $T_o = 10.0$°C. (*a*) Surface plot; (*b*) contour plot. Bumps in the isotherms – indicating upward flows – are revealed as elevations in the surface plot (*a*) and as bright regions in the contour plot (*b*). The plumes that develop at the far left and far right (see figure 4) of the cell are not included in these plots.

Furthermore, the average heights of the isotherms are subtracted to remove the long-term trends seen in figure 5. When displayed as a surface plot (figure 6*a*, for example), the ridges in the surface correspond to the bumps in the isotherm and their associated upward flow. The growth of a plume is revealed as growth of the ridge if followed up and to the left (parallel to the time axis). The same data are displayed as a contour plot (figure 6*b*), from which better estimates can be made of the the precise times for the various phenomena.

Figure 6 shows a space–time plot for the 5°C isotherm (second from bottom in figure 4), which is within the mushy layer throughout the run, except for the first 10 minutes. Plume convection for the right-centre chimney (at $x = 10.7$ cm) is present within the first 10 minutes of the run and grows steadily during the rest of the run. Mushy-layer convection for the left-centre chimney (at $x = 4.9$ cm) is more diffuse early in the run and does not focus into a plume until approximately 30 minutes into the run. A third plume develops at $x = 9.0$ cm, but this plume peaks at approximately 60 min and decays rapidly after that.

The space–time plot for the 9°C isotherm (figure 7) shows that the flow in the liquid region just above the mushy layer is similar in many respects to that in the mushy layer (compare figure 7 with figure 6). As is the case for the 5°C isotherm, the behavior is dominated by the plumes from the left- and right-centre chimneys, along with a plume from a developing chimney at $x = 9.0$ cm that abruptly shuts off after 60 minutes. Closer inspection of figure 7 reveals more activity during the first

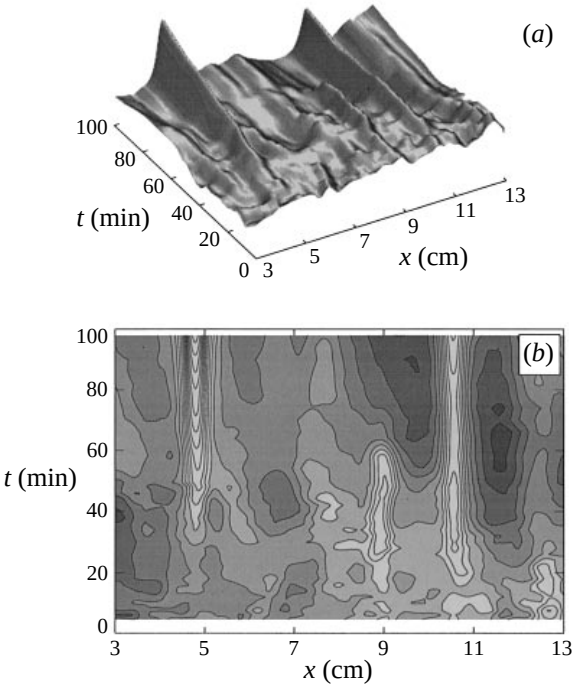

FIGURE 7. Space–time plots of 9°C isotherm (third from bottom in figure 4, in the liquid region above the mush); 10 mm cell thickness, $T_o = 10.0$°C. (*a*) Surface plot; (*b*) contour plot.

20 minutes of the run. These disturbances, which have a shorter average wavelength than the plumes previously discussed, are caused by the boundary-layer mode (salt-finger convection) predicted by Worster (1992). These features are not present for the 5°C isotherm in the mushy layer, consistent with predictions that the boundary-layer mode does not penetrate appreciably into the mushy layer. For the most part, this mode decays away after the first 30–40 min.

The left plume (at $x = 4.9$ cm) first appears in the 9°C isotherm 15 minutes after the start of the run, approximately 10 minutes before the first evidence of a plume at the same location in the 5°C isotherm (compare figure 7*b* with figure 6*b*). This may be an indication that the plume, indeed, is triggered by salt-finger convection in the compositional boundary layer. (On the other hand, it is possible that the plume convection is present in the mushy layer before 25 minutes, but is too weak to be seen as a bump in the isotherm.) Similar comparisons for the $x = 9.0$ and 10.7 cm plumes cannot be made, since they both start within the first 10 minutes, before the 5°C isotherm is covered by the mushy layer.

The evolution of the mushy layer plumes is represented by plotting the height of the bumps in the isotherms (above the average) versus time at the x-location of the plumes. Figure 8 shows these plots for the left- and right-centre plume ($x = 4.9$ and 10.7 cm, respectively) and for the temporary plume at $x = 9.0$ cm. In these plots, comparison is made between the results for the 5 and 9°C isotherms by scaling the bump height (above the average) by the maximum height. This is necessary since flows are weaker in the mushy layer and therefore distortions in the isotherms are smaller than in the liquid region. For the left-centre plume (figure 8*a*), the scaled growth of the bump is almost identical for the 5 and 9°C isotherms (i.e. both within

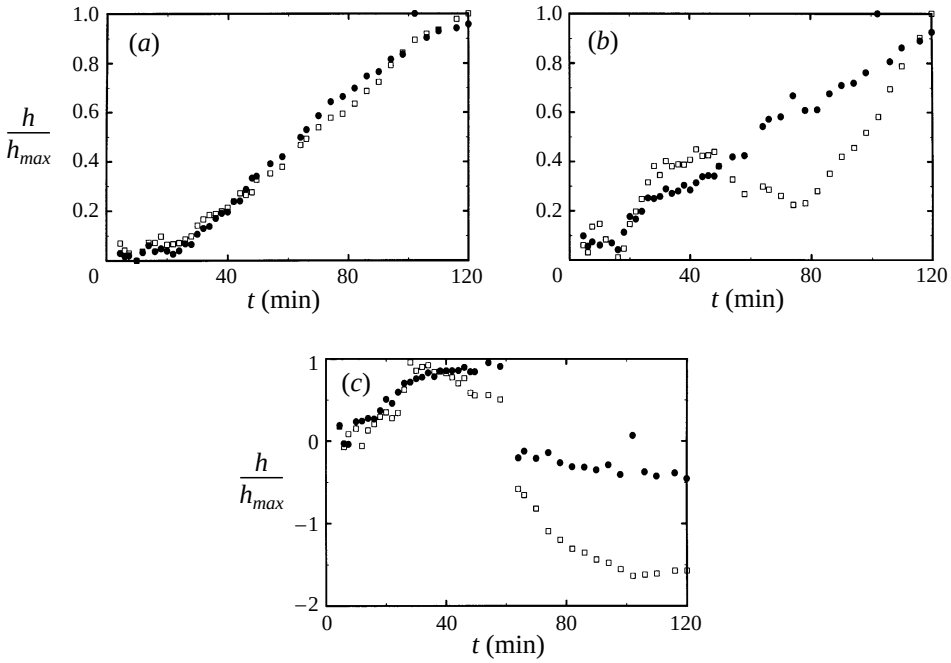

FIGURE 8. Growth and decay of plumes from figures 6 and 7. The height of the bumps in the isotherm above the average is scaled by the maximum height to allow comparision between the data for the 5 and 9°C isotherms, represented by filled circles and open squares, respectively. (*a*) Left-centre plume at $x = 4.9$ cm; (*b*) right-centre plume at $x = 10.7$ cm; (*c*) middle plume at $x = 9.0$ cm.

the mushy and boundary layers), as is expected for the mushy-layer mode, which was shown by Worster (1992) to penetrate simultaneously into both the mushy and liquid regions. (At early times, the scaled 9°C bump is slightly higher than that for the 5°C isotherm, as discussed in the previous paragraph.) The agreement is not as convincing for the right-centre plume (figure 8*b*), due to a significant drop in the height of the 9°C isotherm between 50 and 70 minutes. The time of this drop coincides with the time at which the plume at $x = 9.0$ cm is extinguished (figure 8*c*).

The extinction of the $x = 9.0$ cm plume appears to be evidence of a coarsening (wavelength-selection) mechanism. As can be seen in figure 8(*c*), the plume stops almost completely in less than 2 minutes; in fact, it is replaced by a downflow, seen by the fact that the isotherm drops below the average isotherm height for both the 5 and 9°C isotherms. Chen (1995) has noted that the extinction of chimneys is marked by growth of dendrites into the previously cleared channel. The abruptness of the drop-off in figure 8(*c*) is probably due to the fact that a decrease in the strength of the plume convection decreases the ability of the flow to dissolve dendrites in the channel. The reduced permeability in the channel, in turn, further reduces the plume flow, etc. We are left with the question: what initiates the extinction process, an initial change in the mushy layer flow, or the formation of a small obstruction in the channel (either due to a collapse or to spurious growth of dendrites into the channel)? These questions are resolved by the studies in the 2.0 mm cell, discussed in the next section.

4. Experiments with a 2.0 mm cell

The experiments conducted with a 2.0 mm cell are two-dimensional in the sense that there are no appreciable variations in mush permeability in the cross-gap dimension (thickness). For comparison, the typical chimney width is 5 mm. The fluid flow in the 2.0 mm cell is not strictly two-dimensional, due to no-slip boundary conditions at sidewalls. However, there is no appreciable component of flow in the third (cross-cell) dimension in these cells.

The narrow geometry of the 2.0 mm cell limits chimney formation. Most experiments with this cell result (ultimately) in the formation of only one strong chimney; two chimneys can survive simultaneously in this cell only if they form near opposite ends. Under no circumstances do we ever observe the formation of 4 clean chimneys, as is observed with the 10 mm cell. With the exception of the average number of chimneys formed, though, the behaviour is similar to that of the 10 mm cell. Mushy-layer convection originates within the first 10 minutes, with multiple chimneys forming initially and coarsening to a smaller number after approximately 30–60 minutes. In addition, the mushy-layer mode dominates the flow well after the demise of the boundary-layer mode, as is the case with the 10 mm cell.

The experiments in this section are presented to compare the evolution of convective flows (using TLC imaging) to the development of channels in the mushy layer. Two runs are discussed in this section: a run with the same outer box temperature as the 10 mm run discussed in the previous section ($T_o = 10.0°\mathrm{C}$), as well as one with $T_o = 15.0°\mathrm{C}$ (just slightly below the liquidus temperature).

4.1. *Experiments with* $T_o = 10.0°C$

In a 2.0 mm thick cell, runs with a cool outer box temperature are frequently accompanied by crystallization of NH_4Cl at the edges or along scratches in the sidewalls. In a 10 mm cell, these crystals fall to the bottom before they grow appreciably; in a 2.0 mm cell, however, they can become lodged in the centre of the cell, enabling them to continue growing. In the run shown in figure 9 (with $T_o = 10.0°\mathrm{C}$), crystals form along a seam in the Mylar lamination at the mid-height of the cell. Mushy-layer flows are predicted by Worster (1992), by Amberg & Homsey (1993) and by Emms & Fowler (1994) to be independent of flows in the compositional boundary layer, so we do not expect obstructions much higher in the liquid region to affect processes in the mushy-layer significantly.

The experimental run shown in figure 9 is marked by the early development of two chimneys, one of which dies after 35–40 minutes. Growth of dendrites into the aborted chimney in the centre can be seen in figure 9(*d–f*) (compare with figure 3 from Chen 1995). Space–time plots of the 5°C isotherm (which is below the mush–liquid interface) are shown in figure 10. (Again, only the central region from $x = 3$ to 13 cm is plotted, and the average isotherm heights are subtracted.) The general features of these plots are similar to those for the 10 mm cell (compare with figure 6), the main difference being the smaller number of chimneys in this case. Two plumes are visible: one at $x = 7.7$ cm, which decays after 35 min, and another at $x = 10.9$ cm which grows throughout the run.

Variations in the solid fraction in the 2.0 mm cell are characterized semi-quantitatively from images of the growing NH_4Cl. A solid fraction profile is obtained by summing the intensity of pixels along vertical lines within the mushy layer. The summation does not include variations in the interface height. The averages are subtracted from the profile, which are combined into a space–time plot, as shown in figure 11 for the run of figure 9. There is not a simple linear relation between pixel

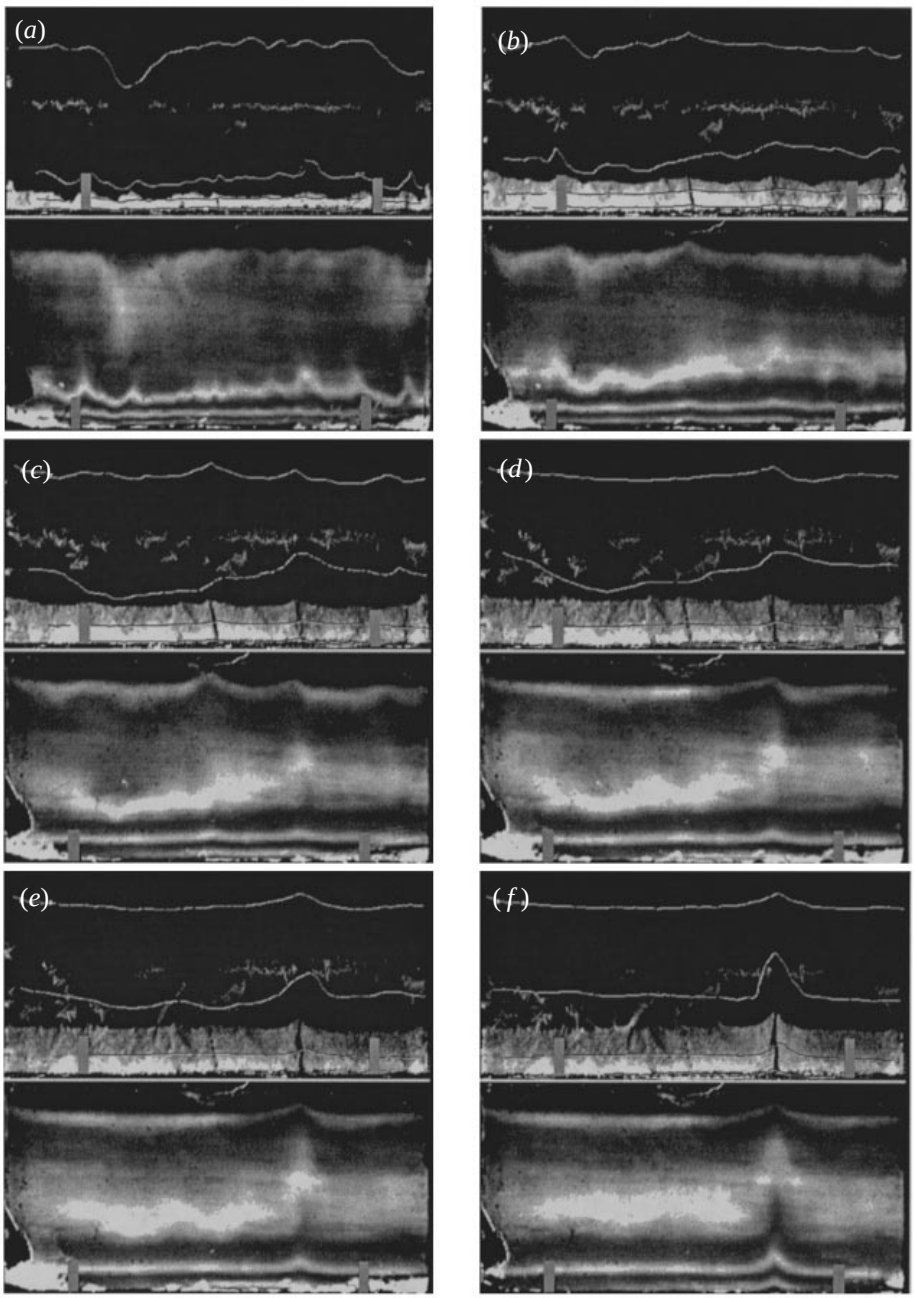

FIGURE 9. Sequence showing solidification in a 2.0 mm thick cell; $T_o = 10.0°C$. In each frame, the top image shows the growing NH_4Cl mushy layer, and the bottom shows the corresponding TLC image. Only four isotherms are visible; the 17°C isotherm is too close to the top plate to be seen. Time after start of run: (*a*) 10 min; (*b*) 20 min; (*c*) 30 min; (*d*) 50 min; (*e*) 70 min; (*f*) 120 min.

intensity and local solid fraction, so the profiles shown in figure 11 are useful primarily for characterizing the time dependence of the chimneys. Contrast in these profiles between the positions with chimneys and those without is diminished by slight tilting of the chimneys. Furthermore, there are appreciable variations in the solid fraction

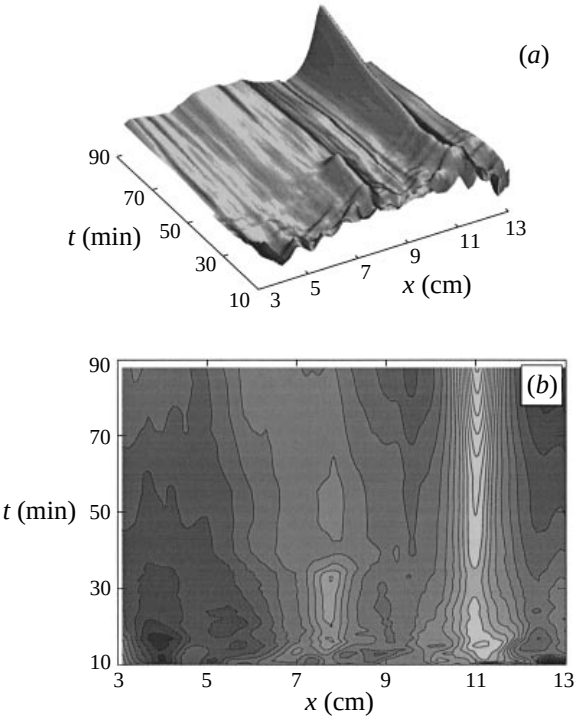

FIGURE 10. Space–time plots of evolution of 5°C isotherm for run shown in figure 9; (second from bottom, inside the mushy layer) 2.0 mm thickness, $T_o = 10.0$°C. (*a*) Surface plot; (*b*) contour plot.

even in regions without chimneys, due possibly to the confining geometry of the 2.0 mm gap thickness.

In figure 11, two chimneys are seen corresponding to the plumes in figure 10: one at $x = 7.7$ cm and the other at $x = 10.9$ cm. The chimney at $x = 7.7$ cm can be seen to start filling in after 35 min, consistent with the drop-off in the flow seen in figure 10. Figure 12 shows the growth and decay of both the plume (solid line) and the channel (dashed line) for the aborted chimney at $x = 7.7$ cm. (The dashed line plots the negative of the scaled solid fraction, so the peak corresponds to the time when the solid fraction in the channel is at a minimum.) The strength of the plume in this chimney peaks at 32 min and drops rapidly after that. The solid fraction reaches its minimum 3 minutes later (at 35 min), after which the channel begins to fill in. The fact that the plume starts to decay before the channel starts filling in indicates that the coarsening process discussed in the previous section is initiated by a change in the mushy-layer flow. Other experiments with the 2.0 mm cell support this conclusion; namely, extinction of a chimney is typically initiated by a change in the mushy layer flows, followed by growth of dendrites into the channel.

Evidence of interaction between plumes can be seen in figure 10. The strength of the plume convection at the $x = 10.9$ cm chimney can be seen to be decreasing shortly before the other plume at $x = 7.7$ cm is extinguished. After the demise of the $x = 7.7$ cm plume at 36 min, the $x = 10.9$ cm plume starts growing again. This is a further indication that chimney extinction is a form of wavelength selection. The coarsening phenomenon observed here is probably related to the growth of the mush. It is well-known that convection rolls/cells typically have width comparable

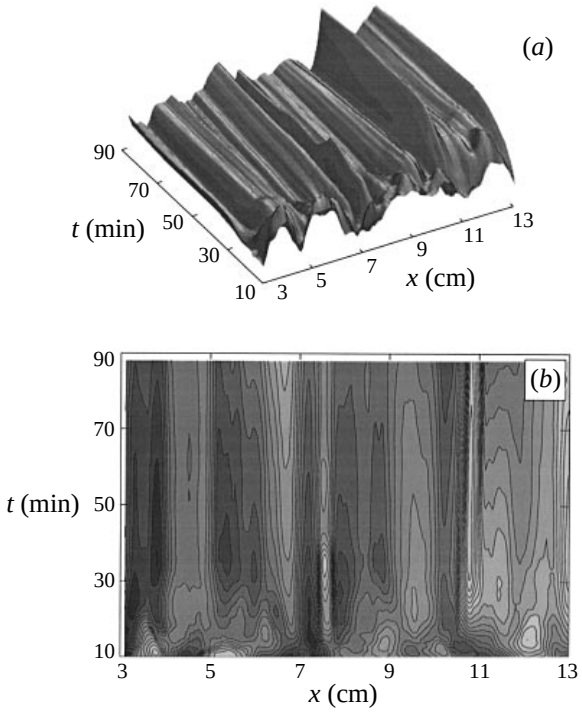

FIGURE 11. Space time plots of the solid fraction profile for the run shown in figure 9; 2.0 mm thickness, $T_o = 10.0°C$. These plots are obtained by summing the intensity vertically in the mushy layer portion of the images and are, therefore, depth-averaged. High points in these plots represent regions of low solid fraction; a large peak therefore represents a chimney. Chimneys initially form at $x = 7.7$ and 10.9 cm. (*a*) Surface plot; (*b*) contour plot.

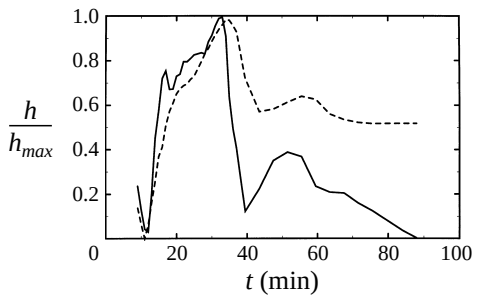

FIGURE 12. Growth and decay of $x = 7.7$ cm plume/channel from figures 10–11. Solid line: height above average of bump in 5°C isotherm, scaled by the maximum. Dotted line: solid fraction in channel (vertically summed intensity), scaled by the minimum such that large values correspond to low solid fractions (i.e. chimneys).

to the depth of the fluid layer (see Normand & Pomeau 1977 for a review). In the case of mushy-layer convection, early in the run, the mush is thin and can presumably support a smaller-wavelength flow. (Note: this assumes that the mush is thick enough to support the mushy-layer mode.) As the mush grows, however, the smaller-wavelength flows become unstable and a unit cell of the flow is eliminated to allow growth of the wavelength. In the case of mushy-layer convection, the elimination of a flow cell results in the extinction of a chimney.

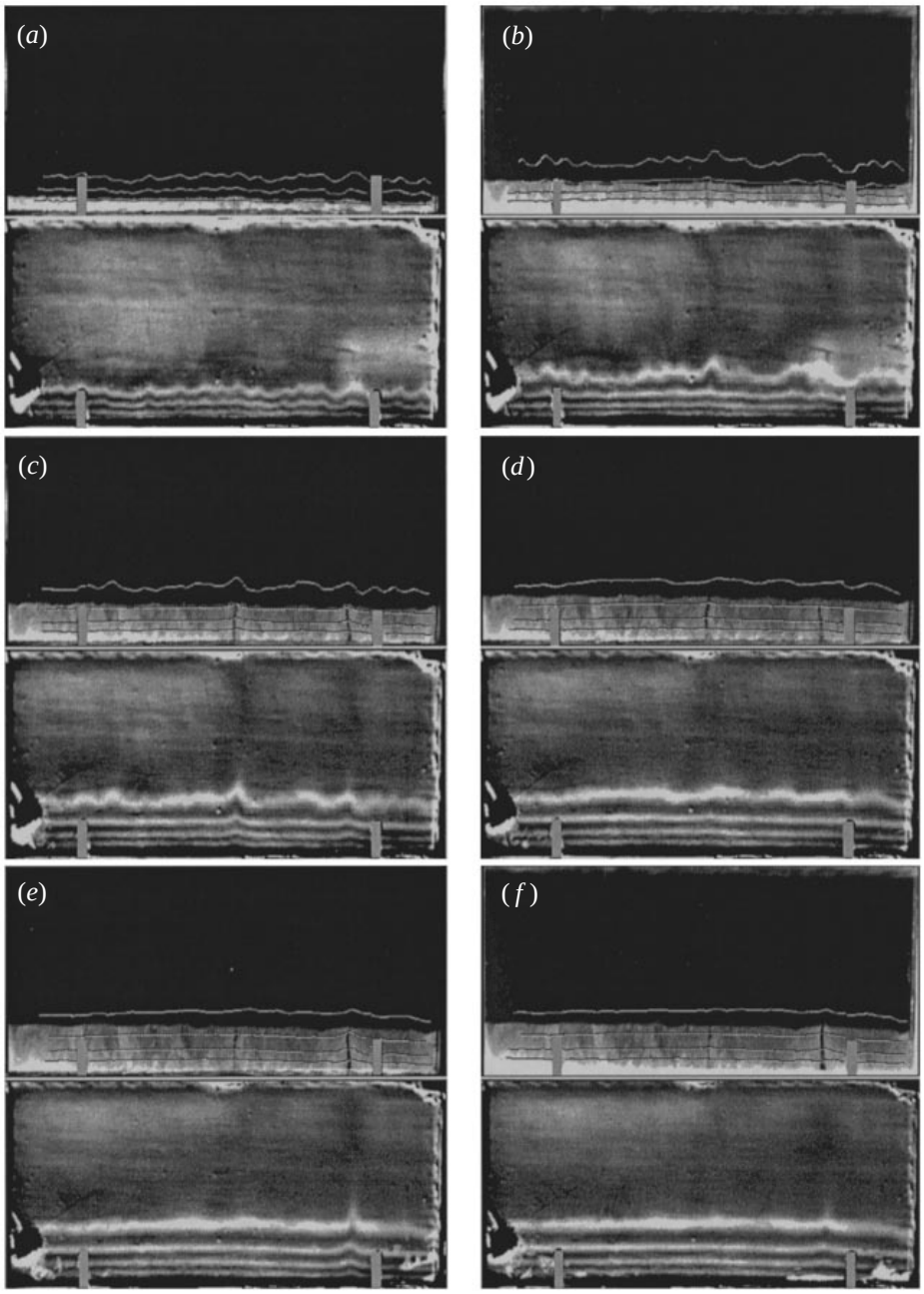

FIGURE 13. Sequence showing solidification in a 2.0 mm thick cell; $T_o = 15.0°C$. In each frame, the top image shows the growing NH_4Cl mushy layer, and the bottom the corresponding TLC image. Time after start of run: (*a*) 10 min; (*b*) 20 min; (*c*) 30 min; (*d*) 50 min; (*e*) 70 min; (*f*) 100 min.

4.2. *Experiments with* $T_o = 15.0°C$*: oscillatory states*

Increasing the outer box temperature eliminates crystallization in the centre of the cell. Other than this, most of the experimental runs with $T_o = 15.0°C$ proceed very much like the run in the previous subsection. Typically, one or two plumes form during the

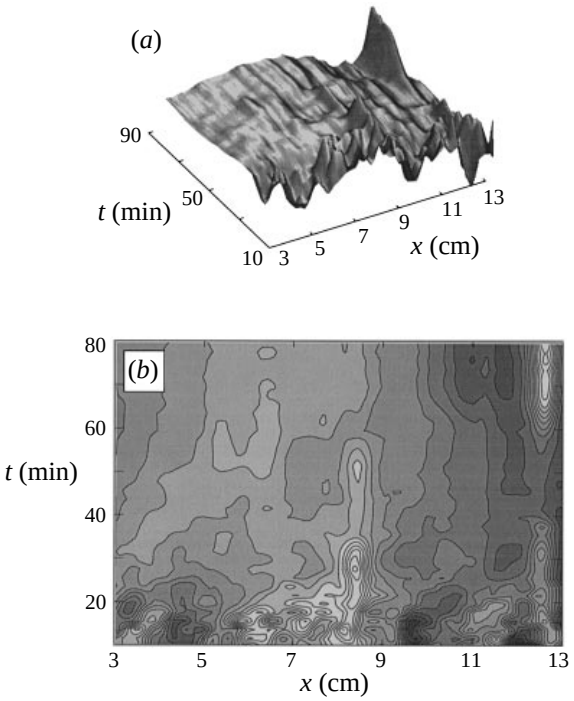

FIGURE 14. Space–time plots of evolution of 9°C isotherm (in the mushy layer) for run shown in figure 13; 2.0 mm thickness, $T_o = 15.0$°C. (*a*) Surface plot; (*b*) contour plot. Oscillations can be observed in the plume intensities, with plumes at $x = 8.5$ cm and $x = 12.7$ cm oscillating out of phase with each other.

first 20–30 minutes and carve out channels. In cases where two plumes form, one of them typically decays, resulting in the growth of dendrites into its channel, similar to the behaviour seen in figures 9–11. Typically, the death of one of the plumes is followed by a pronounced enhancement in the other plume. In some cases, the plume that dies is initially stronger than the one that survives it.

On rare occasions, oscillations are observed between the two plumes and their associated chimneys. In the run shown in figure 13 (with $T_o = 15.0$°C), two plumes/channels start to form, then oscillate back and forth in strength, as seen in the space–time plots for both the 9°C isotherm within the mushy layer (figure 14) and for the solid fraction profile (figure 15). From 20 to 28 min, the left plume (at $x = 8.5$ cm) grows at the expense of the right plume (at $x = 12.7$ cm). The two reverse at 28 min, with the left plume suddenly decaying while the right plume strengthens. The process reverses again at 38 min, with the right plume decaying away almost entirely. Finally, at 50 min, the left plume decays away and the right plume grows rapidly. Note once again that changes in the flow (figure 14) preceed those in the solid fraction (figure 15) by several minutes.

The oscillatory behaviour observed in figures 13–15 is intriguing in the light of recent theoretical predictions of possible oscillatory mushy-layer convection. Linear stability theories proposed by Chen *et al.* (1994) identify an oscillatory state that arises from interactions between the boundary-layer and mushy-layer modes. Under suitable conditions, the two steady modes separate in parameter space with the boundary-layer mode corresponding to small-wavelength disturbances and the mushy-

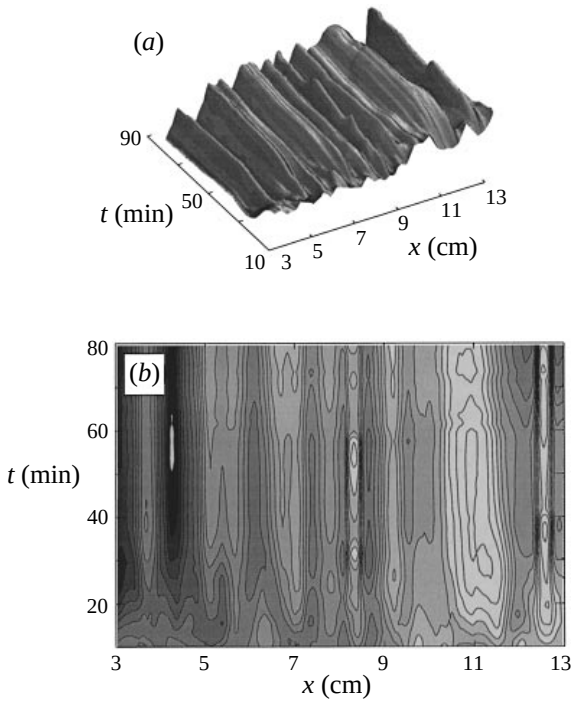

FIGURE 15. Space–time plots of the solid fraction profile for the run shown in figure 13; 2.0 mm thickness, $T_o = 15.0°C$. High points in these plots represent regions of low solid fraction; a peak therefore represents a chimney. Chimneys form at $x = 8.5$ and 12.7 cm and oscillate out of phase with each other. (*a*) Surface plot; (*b*) contour plot.

layer mode corresponding to large-wavelength disturbances. The predicted oscillatory mode is found at intermediate wavelengths in the stability diagram, between the two steady modes. The analysis predicts that the steady modes of convection always become unstable at lower Rayleigh numbers than the oscillatory mode. However, it is plausible that in an experiment, the oscillatory mode could be seen as a transient state if the initial separation of the plumes falls into the band of intermediate wavelengths appropriate for the oscillatory mode. This could explain why the oscillatory states seen experimentally are so rare.

Of course, a careful analysis of the oscillatory states observed in these experiments must use nonlinear approaches, since the experiments are conducted in a regime well above the onset of chimney formation and since the convection is well-developed during the oscillations. For these reasons, the linear stability theory of Chen *et al.* cannot be considered to be a complete explanation of the phenomena observed here.

Nonlinear theories of Anderson & Worster (1996) identified a different oscillatory mode that is intrinsic to the mushy layer. In some circumstances, this oscillatory mode is the most unstable; however, those conditions are not expected to be achievable for laboratory experiments with NH_4Cl, since the concentration ratios for typical experiments NH_4Cl are too high for this instability. Furthermore, the oscillatory mode is predicted to result in lateral motion of the plumes/channels. The oscillations seen in figures 13–15 behave more like standing waves: the locations of the chimneys remain fixed while the amplitude of the plume convection oscillates. However, Anderson & Worster state that nonlinear variations in mushy-layer permeability are likely to lock

the chimneys in place and prevent observation of a travelling wave mode in real systems. It would be interesting to investigate whether consideration of these effects could lead to the prediction of standing wave oscillations.

5. Conclusions

Experimental studies have been made of the growth of ammonium chloride (NH_4Cl) from an aqueous solution in two-dimensional (2.0 mm thickness) and quasi-two-dimensional (10 mm thickness) configurations. A technique using thermochromic liquid crystal (TLC) paints has been used to visualize isotherms both within the mushy layer and in the liquid region. Distortions in these isotherms reveal flows in the system, and space–time plots of the isotherms have been presented to illustrate the initiation, growth and possible decay of these flows.

The results in this paper support the theoretical framework that has been proposed by Worster (1992), Amberg & Homsey (1993), and Emms & Fowler (1994) to describe plume convection and chimney formation in a growing mushy layer. As has been predicted in these studies, the boundary-layer mode is a small-wavelength instability that penetrates negligibly into the mushy layer. The larger-wavelength mushy-layer mode, by contrast, develops simultaneously in the mush and liquid regions, dominating the flow in the system well beyond the time during which most of the excess of NH_4Cl is depleted from the solution.

For both the two-dimensional and quasi-two-dimensional configurations, the long-term spacing of the chimneys appears to be selected by a mechanism in which a closely spaced plumes decays, being replaced in some cases by a down-flow. The reduction and possible reversal of the up-flow enables the growth of dendrites into the channel, closing off the chimney. We have proposed that this coarsening is due to a mechanism related to the increasing mush thickness.

Chimney spacing also depends on the thickness of the experimental cell, with fewer chimneys appearing if the cell thickness is less than the typical chimney width. This may be due to the fact that a narrow geometry effectively reduces the permeability of the mush, restricting the mushy-layer flow in comparison to that with a thicker mush. Experiments are currently in progress to assess the effect of varying mush permeability on the chimney spacing.

An oscillatory mode is observed in runs with the outer box temperature $T_o = 15.0°C$, just below the liquidus temperature of 17°C. This mode, which is rarely seen, behaves like a standing wave: the locations of the chimneys remain fixed, but their amplitudes oscillate out of phase. To our knowledge, this is the first experimental observation of oscillatory behaviour in a growing mush. It is hoped that these results will inspire further nonlinear studies of plume convection and the interactions between chimneys after they have formed.

Care must be taken in extending the results from these experiments to the more general case of growth and decay of chimneys in solidification processes. Clearly, the confining geometry of the 2.0 mm cell affects the process, shown most directly by the lower average number of chimneys that form in this cell. With the 10 mm cell, the cell thickness exceeds the typical plume width; however, even this case cannot be considered to be fully three-dimensional, since the cell thickness is smaller than the typical chimney spacing. Nevertheless, as has been shown in previous experiments (see e.g. Chen 1995), the two-dimensional experiments clearly capture the basic features of chimney evolution found in the larger tanks, even if the quantitative details may differ. In particular, three-dimensional theories of chimney formation have

successfully explained the onset and growth of plume convection in two-dimensional configurations, along with the general movement of fluid within a two-dimensional mushy layer. It is therefore reasonable to postulate that the mechanism for chimney extinction and wavelength selection observed in these experiments applies equally well to those in larger systems, although the final, stable wavelengths will most likely be different. The oscillatory state observed in these experiments may be more difficult to find in larger systems since it appears to be strongly dependent on chimney spacing.

We would like to acknowledge the assistance of Dave Vayda in the construction of the apparatus, and useful discussions with C. F. Chen and D. M. Anderson. Some of the computing equipment for this experiment was funded by a Cottrell College Science Award of Research Corporation (Grant No. CC4002).

REFERENCES

Amberg, G. & Homsey, G. M. 1993 Nonlinear analysis of buoyant convection in binary solidification with application to channel formation. *J. Fluid Mech.* **252**, 79–98.

Anderson, D. M. & Worster, M. G. 1996 A new oscillatory instability in a mushy layer during the solidification of binary alloys. *J. Fluid Mech.* **307**, 245–267.

Chen, C. F. 1995 Experimental study of convection in a mushy layer during directional solidification. *J. Fluid Mech.* **293**, 81–98.

Chen, C. F. & Chen, F. 1991 Experimental study of directional solidification of aqueous ammonium chloride solution. *J. Fluid Mech.* **227**, 567–586.

Chen, F., Lu, J. W. & Yang, T. L. 1994 Convection in directional solidification of aqueous ammonium chloride solutions. *J. Fluid Mech.* **276**, 163–188.

Copley, S. M., Giamei, A. F., Johnson, S. M. & Hornbecker, M. F. 1970 The origin of freckles in unidirectionally solidified castings. *Metall. Trans.* **1**, 2193–2204.

Emms, P. W. & Fowler, A. C. 1994 Compositional convection in the solidification of binary alloys. *J. Fluid Mech.* **262**, 111–139.

Fowler, A. C. 1985 The formation of freckles in binary alloys. *IMA J. Appl. Maths* **35**, 159–174.

Hills, R. N., Loper, D. E. & Roberts, P. H. 1983 A thermodynamically consistent model of a mushy zone. *Q. J. Mech. Appl. Maths* **36**, 505–539.

Huppert, H. E. 1990 The fluid mechanics of solidification. *J. Fluid Mech.* **212**, 209–240.

McDonald, R. J. & Hunt, J. D. 1970 Convective fluid motion within the interdendritic liquid of a casting. *Metall. Trans.* **1**, 1787–1788.

Normand, C. & Pomeau, Y. 1977 Convective instability: A physicist's approach. *Rev. Mod. Phys.* **49**, 581–624.

Sample, A. K. & Hellawell, A. 1984 The mechanisms of formation and prevention of channel segregation during alloy solidification. *Metall. Trans.* A **15**, 2163–2173.

Tait, S., Jahrling, K. & Jaupart, C. 1992 The planform of compositional convection and chimney formation in a mushy layer. *Nature* **356**, 406–408.

Tait, S. & Jaupart, C. 1992 Compositioinal convection in a reactive crystalline mush and melt differentiation. *J. Geophys. Res.* **97**, 6735–6756.

Worster, M. G. 1991 Natural convection in a mushy layer. *J. Fluid Mech.* **224**, 335–359.

Worster, M. G. 1992 Instabilities of the liquid and mushy regions during directional solidification of alloys. *J. Fluid Mech.* **237**, 649–669.

Worster, M. G. 1997 Convection in mushy layers. *Ann. Rev. Fluid Mech.* **29**, 91–122.

Worster, M. G., Anderson, D. M. & Schulze, T. P. 1996 Nonlinear convection in mushy layers. *Proc. 3rd Microgravity Fluid Physics Conf.* (to be published).